Analytical Modeling of Disaster-induced Load Loss for Preventive Allocation of Mobile Power Sources in Urban Power Networks

Zhuorong Wang, Qingxin Shi, Ke Fan, Haiteng Han, Wenxia Liu, and Fangxing Li

Abstract—**Continuous power supply of urban power networks (UPNs) is quite essential for the public security of a city because the UPN acts as the basis for other infrastructure networks. In recent years, UPN is threatened by extreme weather events. An accurate modeling of load loss risk under extreme weather is quite essential for the preventive action of UPN. Considering the forecast intensity of a typhoon disaster, this paper proposes analytical modeling of disaster-induced load loss for preventive allocation of mobile power sources (MPSs) in UPNs. First, based on the topological structure and fragility model of overhead lines and substations, we establish an analytical load loss model of multi-voltage-level UPN to quantify the spatial distribution of disaster-induced load loss at the substation level. Second, according to the projected load loss distribution, a preventive allocation method of MPS is proposed, which makes the best use of MPS and dispatches the limited power supply to most vulnerable areas in the UPN. Finally, the proposed method is validated by the case study of a practical UPN in China.**

Index Terms—**Load loss, fragility model, pre-disaster allocation, mobile power source, urban power network.**

I. Introduction

ENSURING continuous power supply of urban power networks (UPNs) under uncertain operation condition is quite essential for the public security of a city [1]. The concept "power system resilience" is introduced to assess its ability to withstand and recover from significant power outages caused by natural disasters or deliberate attacks [2], [3]. However, enhancing the resilience of UPN is a difficult theoretical and engineering task. First, the power system infrastructure is vulnerable to extreme weather events. For example, in July 2021, the torrential rain in Zhengzhou City, China, caused 1.2 million customers to loose power supply [4]. The electric power utilities dispatched over 400 repair crews and mobile power sources (MPSs) to restore the UPN [5]. Second, the UPN has complex topology and multiple voltage levels, such as high-voltage transmission (HVT), high-voltage distribution (HVD), and medium-voltage distribution (MVD) networks [6], [7]. The component faults at any level may terminate the power delivery path to end users. If $N-k$ line faults occur in extreme weather, HVD and MVD networks are likely to be islanded due to the low redundancy.

In recent years, MPSs are widely used in post-disaster UPN restoration due to its flexible positioning and islanding operation capability [8]. MPSs include truck-mounted diesel generators and truck-mounted modular battery energy storage systems (ESSs) [9]. An efficient post-disaster UPN restoration largely depends on a proper pre-disaster allocation of MPSs because the road network is seriously damaged or flooded in the disaster and long-distance transport of heavy trucks is infeasible or inconvenient [10], [11]. The pre-disaster stage needs an optimal resource allocation under uncertain upcoming fault scenarios. Many research works focus on the pre-disaster allocation in MVD networks. References [11]-[13] formulate the optimal distributed generator (DG) allocation as a tri-level robust programming. Other research works formulate the DG allocation problem in a two-stage stochastic programming [14], [15]. Reference [16] formulates the optimal deployment of ESSs in two-stage stochastic programming. Although the studies focus on the allocation of static DGs and ESSs, the mathematical models are also applicable to that of MPSs. References [17] and [18] formulate the optimal placement of MPSs in the tri-level robust programming and two-stage stochastic programming, respectively.

Despite the rigorous model of pre-disaster allocation of MPS in [17]-[19], the modeling method of load loss uncertainty is limited to an MVD network. This method cannot be directly scaled to urban-level power grids for two reasons. On one hand, the connection relationship between MVD networks and HVD networks is complex. Some distribution feeders are connected to a single substation while others are connected to two substations with a normally-open switch [20]-[22]. On the other hand, The load loss is also caused by the component faults at multi-voltage levels. Therefore, it is a valuable industrial and theoretical problem to pre-allocate

Manuscript received: August 22, 2023; revised: October 29, 2023; accepted: January 14, 2024. Date of CrossCheck: January 14, 2024. Date of online publication: February 2, 2024.

This work was supported by National Natural Science Foundation of China (No. 52307094).

Z. Wang, Q. Shi (corresponding author), K. Fan, and W. Liu are with School of Electrical & Electronics Engineering, North China Electric Power University, Beijing 102206, China (e-mail: iswangzhr@163. com; qshi@ncepu. edu. cn; 120222201107@ncepu.edu.cn; liuwenxia001@163.com).

H. Han is with College of Energy and Electrical Engineering, Hohai University, Nanjing 211100, China (e-mail: hht@hhu.edu.cn).

F. Li is with The University of Tennessee, Knoxville TN 37996, USA (e-mail: fli6@utk.edu).

DOI: 10.35833/MPCE.2023.000591

MPSs based on the spatial distribution of load loss risk. The allocation is naturally determined by the distribution of critical load, multi-voltage-level system topology, and the forecast of disaster impact. A few studies focus on the transmission-level resource allocation and preventive operation of generation units. Reference [23] develops a two-stage robust optimization model to enhance transmission system resilience against ice storms. The first stage coordinates the prepositioned mobile DC de-icing devices (MDIDs) and unit commitment. The second stage coordinates the real-time MDID routing and de-icing schedule. Reference [24] co-optimizes the preparatory schedules of DGs ahead of typhoon considering typhoon-induced outage. Reference [25] adopts a finite-element fragility model of transmission towers and develops a preventive day-ahead security-constrained unit commitment (SCUC) model by using stochastic optimization. Reference [26] presents a day-ahead stochastic tiger dam allocation method to protect power substations against flood events. As far as we know, few literatures have studied the analytical modeling of disaster-induced load loss risk for the preventive allocation of MPSs in UPN.

In summary, the load loss of an UPN results from multiple factors. The external factor includes the intensity of strong wind and rainfall, while the internal factor includes the equipment fragility, the topological redundancy, and spatial load density. It is essential for utility companies to project the spatial distribution of load loss several hours before the disaster so that they can allocate more resources in high-risk regions. As far as we know, there lacks a method to estimate the disaster-induced load loss of the large-scale UPN considering the above factors. Besides, due to the huge number of MVD network nodes, it is not feasible to use sampling-based method, e.g., Monte Carlo simulation, for estimation [14], [15], [27], [28]. This paper proposes analytical modeling of disaster-induced load loss for preventive allocation of MPS in UPNs. The innovations are as follows.

1) A computationally-efficient model is proposed to obtain the spatial distribution of load loss risk in UPN, considering the fault risk of MVD lines, high-voltage overhead lines, and substation transformers. At the MVD level, the expected load loss of each distribution feeder is calculated based on the line fault probability and network connectivity. At the HVD/HVT level, a two-stage path search algorithm is proposed to quantify the impact of high-voltage component fault on the MVD end-users.

2) Based on the projected load loss distribution, we develop a resilience-oriented preventive allocation method of MPSs in the large-scale UPN. This method minimizes the expected load loss during the mid-disaster period via the emergency power supply of MPSs.

The remaining part of this paper is organized as follows. Section II summarizes the topological feature and fragility models of UPNs. Section III proposes the probabilistic modeling of load loss in UPN. Section IV proposes the pre-disaster allocation of MPSs. Section V presents the numerical study. Finally, Section VI concludes the main findings of the paper.

II. Topological Feature and Fragility Models of UPNs

The UPN is a multi-voltage-level network. When specifying the disaster intensity, the load loss percentage of an UPN mainly depends on two factors. One is the topological redundancy of the transmission/distribution system. The other is the fragility model of system components such as overhead lines and substations. This section introduces the topology feature and fragility model of the UPN.

A. Topology Feature

The UPN is a partial transmission network, while it contains many distribution networks. The typical voltage levels of UPN are similar in different countries, as listed in Table I. A typical layout of UPN is presented in Fig. 1.

TABLE I
Typical Voltage Level of UPN

Country	Voltage level (kV)		
	HVT	HVD	MVD
Chinese mainland	220	110	35, 10
USA [6]	115/138, 230	69	26, 13
U.K. [7]	275	132	33, 11
Japan [29]	220	154/77	6.6

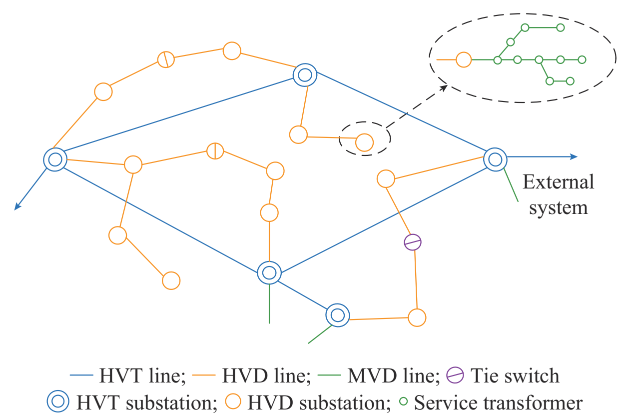

Fig. 1. Typical layout of UPN.

The UPN is a complex network in terms of topology and load composition. From the topology aspect, HVT network constitutes the backbone of the system, which receives the power supply from the external system. The HVD network distributes the power within the city. Since HVT and a few HVD networks are meshed, the $N-1$ fault does not necessarily de-energize any nodes (substations). The MVD network directly connects to service transformers of a building or community. From the load aspect, UPN serves residential load, commercial load, public service load, and transportation load. Above all, we should consider the disaster modeling of both multi-voltage-level networks for the modeling of load loss in UPN.

B. Fragility Model

Fragility model refers to the fault probability of a system component subject to stochastic events. Component faults can be classified into overhead line faults and substation faults. The overhead line fault results from strong wind, in which the distribution poles are damaged and overhand conductors are likely to be short-circuited. The substation fault results from flood, in which the main transformer is inundated [30]. In some coastal areas, the typhoon, accompanied with strong rainfall, is likely to cause both overhead line faults and substation faults [31]. Therefore, this paper considers the typhoon and flood scenarios as examples for the pre-disaster allocation.

The fragility model of overhead lines is determined by wind speed, wind direction, and landing path. The Batts model [32] is adopted in this paper. The wind speed at each point of the typhoon wind field is expressed as:

$$v=\begin{cases} v_{R\max}\left(\dfrac{R_{\max}}{R}\right)^{\alpha} & R>R_{\max} \\ v_{R\max}\dfrac{R_{\max}}{R} & R\le R_{\max} \end{cases} \tag{1}$$

$$R_{\max}=\exp(-0.1239(\Delta p(t))^{0.6}+5.1) \tag{2}$$

$$\Delta p(t)=\Delta p_0-0.675(1+\sin\varphi)t \tag{3}$$

$$v_{R\max}=0.865(0.865\sqrt{\Delta p(t)}-0.5R_{\max}f)+0.5v^T \tag{4}$$

where $R_{\max}$ is the radius corresponding to the maximum wind speed; R is the radius from the center of the typhoon; $v_{R\max}$ is the maximum wind speed; α is the empirical coefficient ranging from 0.5 to 0.7; $\Delta p(t)$ is the central pressure difference after the typhoon landing at t; Δp_0 is the pressure difference between the center of the typhoon and the periphery of the cyclone before typhoon landing; φ is the angle between the movement direction of typhoon and the coastline at the time of typhoon landing; t is the time after the typhoon lands; v^T is the typhoon moving speed; and f is the Coriolis force of the earth's rotation.

1) Fault Probability of High-voltage Overhead Lines

In this paper, an exponential function is used to fit the fault probability of poles and wind speed [33]. The expression is shown as:

$$\lambda_p^h=\begin{cases} 0 & 0<v_p^R<v^H \\ 1-\exp\left(-\dfrac{\exp(K_1(v_p^R-v^H))}{1-\exp(K_1(v_p^R-v^H))}\right) & v^H\le v_p^R\le v_{\max}^H \\ 1 & v_p^R>v_{\max}^H \end{cases} \tag{5}$$

$$\lambda_i^H=1-\prod_{p=1}^{N^P}\lambda_p^h \tag{6}$$

where λ_p^h is the fault probability of the pole p; K_1 is an empirical coefficient; v_p^R is the maximum wind speed sustained by the pole p; v^H is the designed wind speed tolerance of the high-voltage pole; $v_{\max}^H$ is the maximum wind speed that the high-voltage overhead line can withstand; λ_i^H is the fault probability of the high-voltage overhead line i; and N^P is the number of poles of a high-voltage overhead line.

2) Fault Probability of MVD Overhead Lines

The wind speed across the distribution feeder can be assumed identical because the size is much smaller than the typhoon eye. Therefore, the fault rate of the overhead line can be determined by the maximum wind speed [34].

$$\lambda_i^M=\begin{cases} 0 & 0<v_i^R<v^M \\ \Delta l\cdot\exp\left(K_2\dfrac{v_i^R}{v^M}-K_3\right) & v^M\le v_i^R\le v_{\max}^M \\ 1 & v_i^R>v_{\max}^M \end{cases} \tag{7}$$

where λ_i^M is the fault probability of the medium-voltage overhead line i; K_2 and K_3 are the empirical coefficients, and $K_2=11$, $K_3=18$; Δl is the length of the overhead line i; v_i^R is the maximum wind speed sustained by the medium-voltage overhead line i; v^M is the designed wind speed tolerance of the medium-voltage overhead line; and $v_{\max}^M$ is the maximum wind speed that the medium-voltage overhead line can withstand.

3) Fault Probability of Substations

Typhoon is usually accompanied by torrential rains. The common ways in which storms affect substations can be categorized into two types. The first is that excessive rainfall will cause a string short-circuit fault in the insulator of substation branch column. The second is the local flood that makes the equipment in the substation to be submerged in water, causing a total shutdown of the substation [35]. The rain flush probability of the insulator λ_e^F is given by (8).

$$\lambda_e^F=\begin{cases} 0 & \delta_{water}<2\ \text{mm/min} \\ 0.5 & 0.9\le r\le 1 \\ 1 & r<0.9 \end{cases} \tag{8}$$

where δ_{water} is the effective water (rain) intensity; and r is the AC rain flash voltage coefficient of insulator string.

The model parameters are calculated by (9)-(12).

$$r=A_p\delta_{water}^{-a} \tag{9}$$

$$\delta_{water}=\max\{y_2,y_3\} \tag{10}$$

$$\lambda_e^V=\begin{cases} 0 & R^F<R_0^F \\ \exp\left(c\dfrac{R^F}{R_0^F}-d\right) & R_0^F\le R^F\le 1.5R_0^F \\ 1 & R^F>1.5R_0^F \end{cases} \tag{11}$$

$$R^F=y_1+y_2T_1+y_3T_2-(x_1+x_2)(T_1+T_2) \tag{12}$$

where A_p, c, and d are the computer factors; a is the characteristic index indicating the effect of effective rain intensity on AC rain flash voltage of insulator string; y_1, y_2, and y_3 are the real-time water level in the substation, real-time rainfall value, and forecasted rainfall value, respectively; R^F and R_0^F are the effective rainfall and standard flood protection precipitation during the recurrence period specified by the flood protection standard of the substation, respectively; x_1 and x_2 are the discharge volume of the internal drainage pump of the substation and the amount of natural flow in the substation, respectively; and T_1 and T_2 are the real-time rainfall time duration and forecasted precipitation duration, respectively.

The combined risk probability of the substation λ_e^S under heavy rainfall conditions is defined as:

$$\lambda_e^S=1-(1-\lambda_e^F)(1-\lambda_e^V) \tag{13}$$

III. Probabilistic Modeling of Load Loss in UPN

The probabilistic modeling of load loss indicates calculating the expected value of load shedding under uncertain fault scenarios. First, a sufficient set of independent fault scenarios can be generated by using stochastic sampling algorithms, e.g., Monte Carlo simulation, and calculating the average load loss [14], [15]. The expected value is given by (14).

$$E=\sum_{s\in S}\Delta P_s \tag{14}$$

where E is the excepted load loss; s and S are the index and set of stochastic fault scenarios, respectively; and ΔP_s is the load loss for scenario s.

If multiple scenarios with different fault locations result in the same load loss, we can cluster them and use one scenario to represent this group [15]. Then, a large group of scenarios is reduced to a small group. Equation (14) is transferred to (15).

$$E=\sum_{s\in S}\varphi_s\Delta P_s \tag{15}$$

where φ_s is the component fault probability for scenario s.

Second, the load loss can be directly calculated according to the power supply path and component fault probability [20]. Considering the radial topology of MVD network, it is feasible to directly generate the fault scenario set and calculate the expected value by using (15). This section proposes an analytical method. At the MVD level, an analytical method is established to aggregate the load loss at the substation level. At the HVD level, a two-stage path search algorithm is proposed to describe the disaster-induced load loss uncertainty.

A. Load Loss of MVD Network

Generally, a substation supplies multiple distribution feeders (divided by transformers).

1) Topology Reduction

In a distribution feeder, each service transformer can be regarded as a node. Then, the feeder is a collection of load nodes and switch, as shown in Fig. 2(a). If any branch (indicated by ①-⑧) between the two sectionalizing switches (SSs) fails, the SS isolates this sub-section of the feeder. We set the branch equipped with SS as the boundary and combine all nodes between two SSs. Therefore, the structure of distribution networks is simplified, as shown in Fig. 2(b).

2) Power Supply Path and Influence Node Matrix

In a radial network, the power supply path of a load node is unique. Thus, the relation between faulty branches and resultant load loss can be expressed by the power supply path and influence node matrix (denoted as PSILM) [20]. As shown in Fig. 3, load nodes are numbered according to the depth first search (DFS) algorithm to make the matrix more readable [36]. PSILM is generated as follows. First, generate node-branch incidence matrix $\boldsymbol{A}$ according to the principle: $A_{ki}=1$ if node k is the starting node of branch i; $A_{ki}=-1$ if node k is the ending node of branch i; $A_{ki}=0$ if node k does not belong to branch i. Second, delete the first row of $\boldsymbol{A}$ (denoted as $\bar{\boldsymbol{A}}$) and obtain the inverse $\bar{\boldsymbol{A}}^{-1}$.

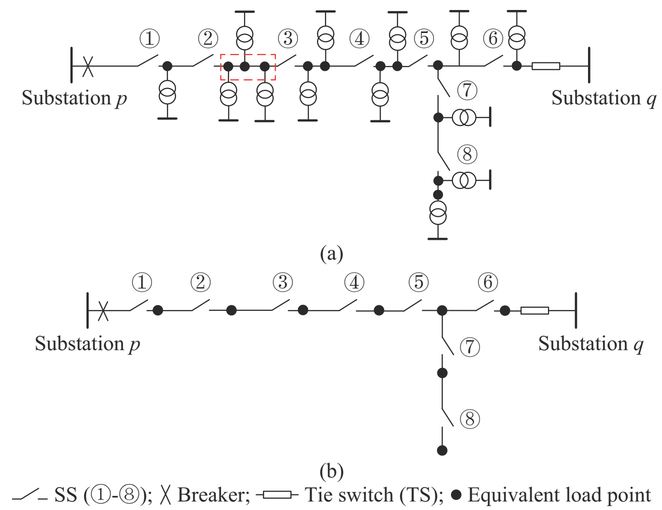

Fig. 2. Simplification of distribution network topology. (a) Original network. (b) Simplified network.

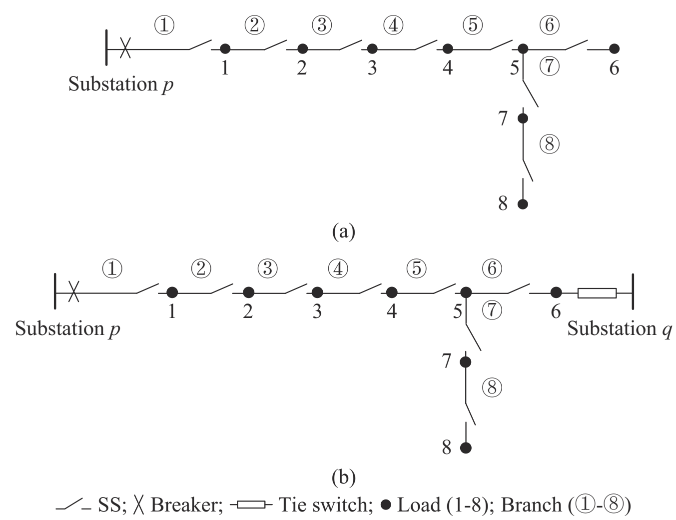

Fig. 3. Layout of typical distribution feeder. (a) Single power source. (b) Double power source.

Third, obtain PSILM $\boldsymbol{B}$ by calculating the absolute value of each component of $\bar{\boldsymbol{A}}^{-1}$. Therefore, $B_{ik}=1$ indicates that load node k will be affected (deenergized) if branch i is faulty; otherwise, $B_{ik}=0$. An example of matrix generation is shown in Fig. 4. Each row represents the set of load nodes being affected by a branch fault, while each column represents the set of branches in the power supply path of a node. For example, if branch 2 fails, load nodes {2, 3, 4, 5, 6, 7, 8} will be influenced. Also, the power supply path of node 7 is {1, 2, 3, 4, 5, 7}.

$$\begin{array}{c|cccccccc}
 & ① & ② & ③ & ④ & ⑤ & ⑥ & ⑦ & ⑧ \\
\hline
\cancel{0} & \cancel{1} & \cancel{0} & \cancel{0} & \cancel{0} & \cancel{0} & \cancel{0} & \cancel{0} & \cancel{0} \\
1 & -1 & 1 & 0 & 0 & 0 & 0 & 0 & 0 \\
2 & 0 & -1 & 1 & 0 & 0 & 0 & 0 & 0 \\
3 & 0 & 0 & -1 & 1 & 0 & 0 & 0 & 0 \\
4 & 0 & 0 & 0 & -1 & 1 & 0 & 0 & 0 \\
5 & 0 & 0 & 0 & 0 & -1 & 1 & 1 & 0 \\
6 & 0 & 0 & 0 & 0 & 0 & -1 & 0 & 0 \\
7 & 0 & 0 & 0 & 0 & 0 & 0 & -1 & 1 \\
8 & 0 & 0 & 0 & 0 & 0 & 0 & 0 & -1
\end{array}
\xrightarrow{\text{Take absolute value of inverse}}
\begin{array}{c|cccccccc}
 & 1 & 2 & 3 & 4 & 5 & 6 & 7 & 8 \\
\hline
① & 1 & 1 & 1 & 1 & 1 & 1 & 1 & 1 \\
② & 0 & 1 & 1 & 1 & 1 & 1 & 1 & 1 \\
③ & 0 & 0 & 1 & 1 & 1 & 1 & 1 & 1 \\
④ & 0 & 0 & 0 & 1 & 1 & 1 & 1 & 1 \\
⑤ & 0 & 0 & 0 & 0 & 1 & 1 & 1 & 1 \\
⑥ & 0 & 0 & 0 & 0 & 0 & 1 & 0 & 0 \\
⑦ & 0 & 0 & 0 & 0 & 0 & 0 & 1 & 1 \\
⑧ & 0 & 0 & 0 & 0 & 0 & 0 & 0 & 1
\end{array}$$

Fig. 4. An example of matrix generation.

Some distribution lines in the UPN are connected to a single substation, while others are connected to two substations through a normally-open TS. Therefore, the power supply mode of these lines can be classified into two modes.

1) Mode a: the line is normally energized by only one substation. An example is shown in Fig. 3(a).

2) Mode b: the line is energized by one substation with one backup substation. An example is shown in Fig. 3(b).

3) Power Supply Mode a

Based on matrix $\boldsymbol{B}$ and the vector of branch fault probability, the excepted value of load loss of feeder l is calculated by (16)-(18).

$$\Delta P_{i,l}^{Ta}=\sum_{k=1}^{M}B_{ik}(P_k-P_k^{DG})\quad \forall i\in\Omega_l^B \tag{16}$$

$$\varphi_{i,l}=\lambda_{i,l}^{L}\prod_{k=1,k\neq i}^{M}[B_{ik}(1-\lambda_{i,l}^{L})+(1-B_{ik})]\quad \forall i\in\Omega_l^B,\forall k\in\Omega_l^N \tag{17}$$

$$E_l^{Ta}=\sum_{i=1}^{M}\varphi_{i,l}\Delta P_{i,l}^{Ta}\quad \forall l\in\Omega_L \tag{18}$$

where $\Delta P_{i,l}^{Ta}$ is the load loss value in the case of Mode a; M is the number of branches; k is the index of load node; i is the index of branches; P_k is the load demand of node k; P_k^{DG} is the distributed energy source on node k; $\varphi_{i,l}$ is the probability that branch i is faulty and its upstream branch is normal; $\lambda_{i,l}^{L}$ is the probability of branch i; E_l^{Ta} is the excepted load loss of Mode a; Ω_l^B and Ω_l^N are the sets of load node and branches within feeder l, respectively; and Ω_L is the set of distribution feeders.

Equation (16) calculates the load loss of each $N-1$ fault scenario. Equation (17) represents the probability in which the adjacent upstream branch i is faulty and other upstream branches are normal. The downstream branches are deenergized whether they are damaged. Therefore, all fault scenarios can be represented by the $N-1$ fault scenario. The number of fault scenarios is reduced from 2^M to M.

4) Power Supply Mode b

The fault scenarios in double-source feeder are more complex than those in single-substation. To simplify the calculation process, we aggregate the sub-branch, e.g., branches {7, 8} in Fig. 5, into one load node in the first step and add it back in the second step. The fault scenarios can be classified into three types.

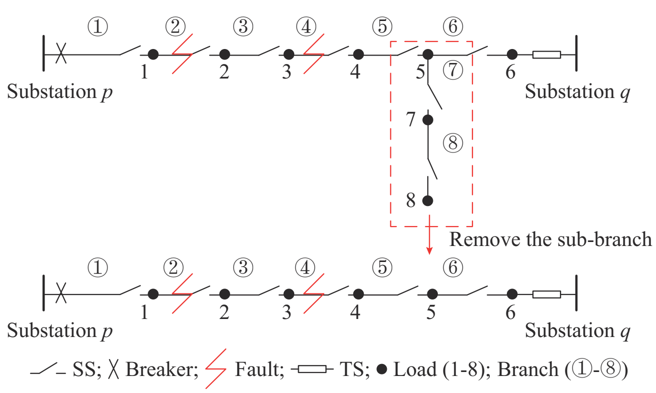

Fig. 5. Simplification of two-substation system.

1) The load node is not energized. Thus, load nodes do not supply power whether sub-branches are normal or not.

2) The load node is energized and all sub-branches are normal. All load nodes can supply power in this case.

3) The load node is energized and at least one sub-branch is faulty. This fault scenario is similar to single-source case.

If branch i is directly connected to substation p, e. g., branch 1, and substation q is the back-up source, $M-1$ fault does not affect the power supply of any nodes. Similarly, if node k is connected to the substation q by SS, no branch fault can affect the power supply of node k. Hence, the PSILM of Mode b can be modified as follows. First, delete the k^{th} row and i^{th} column and inverse the matrix. Second, add "0" in the i^{th} row and k^{th} column to obtain the PSILM of substation q. The example is shown in Fig. 6(a).

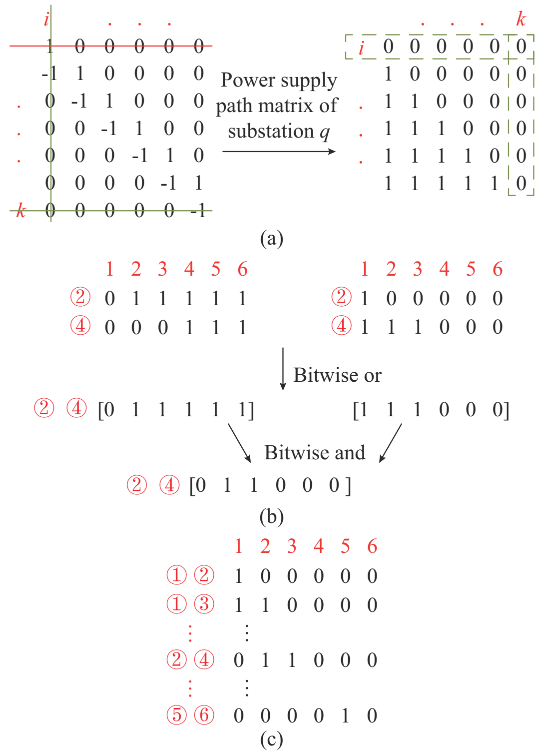

Fig. 6. Correlation matrix and formation process. (a) Power supply and influence load matrix of substation q. (b) Operation process. (c) Relationship matrix.

In Mode b, only $M-2$ faults need to be considered because it includes all other load loss possibilities of $M-k$ faults when $2<k\leq M$. Furthermore, the set of nodes affected by the simultaneous faults of branches i and j is the intersection of two sets affected by the separate faults of branches i and j in single-source case, respectively. Then, we can obtain the set of affected nodes of substation p, S_{pij}, via the intersection set of two branch faults. It is represented by the i^{th} row of bitwise and the j^{th} row in PSILM. Similarly, the set of affected load nodes S_{qij} can be obtained when only the substation q is supplied. Therefore, the load nodes $k\in S_{pij}\cap S_{qij}$ are affected when the TS is closed and there is no fault in both substations. An example of the operation process is shown in Fig. 6(b). When branches 2 and 4 are faulty, the affected

node set is {2, 3} by taking the intersection. The calculation process can be expressed as:

$$\boldsymbol{C} = \boldsymbol{C}^{Tp} \circ \boldsymbol{C}^{Tq} \tag{19}$$

where $\circ$ is the symbol for multiplying the elements of a matrix by bits; $\boldsymbol{C}$ is the relationship matrix; and $\boldsymbol{C}^{Tp}$ and $\boldsymbol{C}^{Tq}$ are the correlation matrices when the power supplies are p and q, respectively.

The total number of $M-2$ fault scenarios on feeder l is $M_l^F = \mathrm{C}_N^2$, where N equals N_l^b, which is the number of load nodes after removing sub-branches. Since the branch fault condition affecting the power supply to the load node can be derived from the above operation, we can use a structure similar to $\boldsymbol{B}$ to form $\boldsymbol{C}$, as shown in Fig. 6(c). Similarly, the column of $\boldsymbol{C}$ represents the load node. $C_{mk}=1$ indicates load node k will be affected (deenergized) if the branch fault condition is m; otherwise, $C_{mk}=0$. Each row element indicates the condition of the node affected by the branch fault. Finally, the expected load loss of the main branches on feeder l E_l^{Tcm} is calculated by (20)-(22).

$$\Delta P_{i,l}^{Tb} = \sum_{k=1}^{M} C_{ik}\left(P_k - P_k^{DG}\right) \quad \forall i \in \Omega_l^B \tag{20}$$

$$\varphi_{m,l} = \prod_{\substack{i=f_m^{\max},\\ i=f_m^{\min}}} \lambda_{i,l}^L \prod_{\substack{i>f_m^{\max},\\ i<f_m^{\min}}} \left(1-\lambda_{i,l}^L\right) \quad \forall i \in \Omega_l^{BM}, \forall m \in \Omega_l^{FS} \tag{21}$$

$$E_l^{Tbm} = \boldsymbol{\Phi}_l^{\mathrm{T}} \Delta \boldsymbol{P}_l^{Tb} \quad \forall l \in \Omega_L \tag{22}$$

where $\Delta P_{i,l}^{Tb}$ is the load loss value in the case of Mode b; m is the index of fault situation; $\varphi_{m,l}$ is the probability of the fault situation m; $f_m^{\max}$ and $f_m^{\min}$ are the maximum and minimum nodes in fault situation m, respectively; $\boldsymbol{\Phi}_l$ is the probability matrix of fault situation; $\Delta \boldsymbol{P}_l^{Tb}$ is the matrix of load loss; Ω_l^{BM} is the set of branches after removing the sub-branch; Ω_l^{FS} is the set of fault situations; and E_l^{Tbm} is the expected load loss of the main branch on feeder l.

The fault situations of node with sub-branch are divided into two sets, which are represented by $\Omega_{l,k}^F$ and $\Omega_{l,k}^U$, respectively. Therefore, the expected load loss is calculated by:

$$E_l^{Tbs} = \sum_{sl \in \Omega_l^{SL}} \left[\sum_{m \in \Omega_{l,k}^F} \left(\varphi_{l,m} \sum_{sk \in \Omega_{sl,k}^N} P_{sk} \right) + \sum_{m \in \Omega_{l,k}^U} \varphi_{l,m} E_{sl}^{Ta} \right] \tag{23}$$

where E_l^{Tbs} is the expected load loss of the sub-branches on feeder l; Ω_l^{SL} is the set of load nodes with sub-branches on feeder l; and $\Omega_{sl,k}^N$ is the set of load nodes on branch sl.

Above all, the excepted load loss of Mode b consists of those caused by main branch faults and sub-branch faults, respectively:

$$E_l^{Tb} = E_l^{Tbm} + E_l^{Tbs} \quad \forall l \in \Omega_L \tag{24}$$

where E_l^{Tb} is the excepted load loss of Mode b.

The expected load loss of the MVD network is calculated by adding the expected load loss of feeders under the possible uncertain fault of high-voltage substation e.

$$\Delta P_e^{MVT} = \sum_{l \in \Omega_e^L} E_l \quad \forall e \in \Omega_{EN} \tag{25}$$

where Ω_{EN} is the set of high-voltage substations; and Ω_e^L is the set of feeders for substation e.

B. Load Loss of High-voltage Network

The analytical model in Section III-A aggregates the load loss at the MVD network. From the perspective of UPN, the expected load loss not only depends on the fault of MVD networks, but also depends on the fault of upstream high-voltage networks, which acts as the power supply path from power plants to end-users. Therefore, it is necessary to model the fault probability of HVD/HVT lines. Considering the large number of feeders in a city, the proposed analytical method for computing expected load loss is sufficiently accurate for pre-disaster allocation.

1) Supply Path Search Algorithm

In this part, the DFS algorithm is adopted to power supply path from the EHV substation and the HVD substation. The procedure to find the power supply path of the target node is as follows.

1) Visit its first child node of the source node and push it into stack.

2) Find the first child node of the topmost node on the stack, repeat this step until the final destination node is found, and record the power supply path. Then, pop the final destination node and continue to search other power supply paths. In other words, visit the next sibling of the parent node. If the parent node is not adjacent to the next sibling, the next sibling of the grandfather node is visited.

3) Repeat the above steps until all nodes are visited and all power supply paths are recoded.

2) Expected Load Loss Calculation

The expected load loss can be calculated in a method similar to that of MVD networks. Due to the complexity of UPN, the result obtained from direct calculation of all nodes to source nodes is complex. The expected load loss is calculated in two stages. As shown in Fig. 7, the power supply path from EHV substation to HVT substation and from HVT substation to HVD substation are regarded as two stages, respectively. Then, the expected load loss is obtained. If the substation fails, all the loads of this substation are outage, which does not affect the power supply of its downstream unfaulty substation. Similarly, when the upstream substation fails, it does not affect the power supply of the substation node. Therefore, the reduction formula of fault probability is shown by (26)-(30).

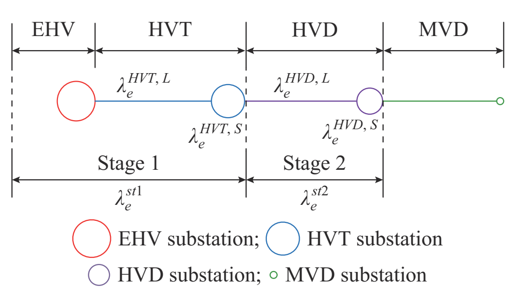

Fig. 7. Two-stage path search algorithm.

$$\lambda_e^{HVT,L} = \prod_{c \in \Omega_e^c} \left(1 - \prod_{i \in \Omega_{k,c}} \left(1-\lambda_i^H\right)\right) \quad \forall e \in \Omega_{EN}^{HVT} \tag{26}$$

$$\lambda_e^{HVD,L} = \prod_{c \in \Omega_e^c}\left[1 - \prod_{i \in \Omega_{k,c}}(1-\lambda_i^H)\right] \quad \forall e \in \Omega_{EN}^{HVD} \tag{27}$$

$$\lambda_e^{st1} = 1-(1-\lambda_e^{HVT,S})(1-\lambda_e^{HVT,L}) \quad \forall e \in \Omega_{EN}^{HVT} \tag{28}$$

$$\lambda_e^{st2} = 1-(1-\lambda_e^{HVD,S})(1-\lambda_e^{HVD,L}) \quad \forall e \in \Omega_{EN}^{HVD} \tag{29}$$

$$\lambda_e = \prod_{w \in \Omega_e^{pe}}[1-(1-\lambda_w^{st1})(1-\lambda_e^{st2})] \quad \forall w \in \Omega_{EN}^{HVT}, \forall e \in \Omega_{EN}^{HVD} \tag{30}$$

where w is the index of high-voltage substation; λ_i^H and λ_i^L are the fault probabilities of HVT and HVD lines, respectively; $\lambda_e^{HVT,L}$ and $\lambda_e^{HVD,L}$ are the equivalent fault probabilities of HVT and HVD lines, respectively; λ_e^{st1} and λ_e^{st2} are the equivalent fault probabilities of stage 1 and stage 2, respectively; $\lambda_e^{HVT,S}$ and $\lambda_e^{HVD,S}$ are the fault probabilities of HVT and HVD substations, respectively; λ_e is the equivalent fault probability of HVD network; $\Omega_{k,c}$ is the set of power supply lines passed by power supply c; Ω_e^C is the set of power supply for substation e; and Ω_e^{pe} is the set of power sources that have power supply paths to substation e.

Equations (26) and (27) represent the overall fault probability of the high-voltage overhead line. Equations (28) and (29) calculate the fault probability of the HVT and HVD supply paths, respectively. Finally, the fault probability of the whole supply path is calculated by (30). Therefore, the expected load loss of substation e and the total expected load loss are formulated as (31) and (32), respectively.

$$\Delta P_e^{HVD} = \lambda_e(P_e - \Delta P_e^{MVT}) \quad \forall e \in \Omega_{EN} \tag{31}$$

$$P_e^L = \Delta P_e^{MVT} + \Delta P_e^{HVT} \quad \forall e \in \Omega_{EN} \tag{32}$$

where ΔP_e^{HVD} is the expected load loss of HVD network; and P_e^L is the total excepted load loss.

C. Summary

The overall technical framework is shown in Fig. 8. In the MVD network, the expected load loss of each feeder is estimated based on the power supply path and load distribution. In the HVT/HVD network, a two-stage path search algorithm is used to calculate the expected load loss of HVD network. The combination effect of line faults of multi-voltage-level UPN is a representation of the overall load risk, which provides the preventive operation with essential guidance.

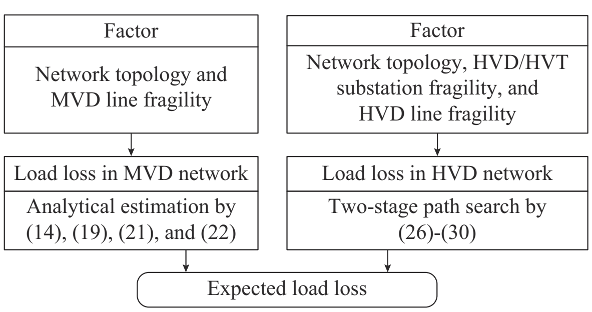

Fig. 8. Technical framework.

IV. Pre-disaster Allocation of MPS

This section proposes a pre-disaster allocation of MPSs in order to reduce the expected cost of load loss. Meanwhile, the post-disaster re-dispatch of MPSs is minimized. The MPSs consist of mobile emergency generators (MEGs), mobile energy storage systems (MESSs), and electric buses (EBs). Under complex disaster-induced load loss uncertainty, a mixed-integer linear programming model is proposed based on the expected value of load loss calculated in Section III. The objective function (33) aims to minimize the cost of load loss and MPS placement within the city.

$$\min \sum_{e \in \Omega_{EN}} (c_e^M \alpha_e^M + c_e^D \beta_e^D + c_e^E \gamma_e^E + c_e^L \Delta P_e^L) \tag{33}$$

where c_e^M, c_e^D, and c_e^E are the unit output costs of MEG, MES, and EB, respectively; c_e^L is the cost reduction per unit load; α_e^M, β_e^D, and γ_e^E are the dispatchable MEG, MESS, and EB, respectively; and ΔP_e^L is the load loss after the deployment of MPS groups.

The constraints are given by (34)-(41).

$$\sum_{e \in \Omega_{EN}} \alpha_e^M \le N^M \tag{34}$$

$$\sum_{e \in \Omega_{EN}} \beta_e^D \le N^D \tag{35}$$

$$\sum_{e \in \Omega_{ENE}} \gamma_e^E \le N^E \tag{36}$$

$$0 \le P_e^M \le \alpha_e^M \bar{P}_e^M \quad \forall e \in \Omega_{EN} \tag{37}$$

$$0 \le P_e^D \le \beta_e^D \bar{P}_e^D \quad \forall e \in \Omega_{EN} \tag{38}$$

$$0 \le P_e^E \le \gamma_e^E \bar{P}_e^E \quad \forall e \in \Omega_{ENE} \tag{39}$$

$$\Delta P_e^L = P_e^L - P_e^M - P_e^D - P_e^E \quad \forall e \in \Omega_{EN} \tag{40}$$

$$0 \le P_e^M + P_e^D + P_e^E \le \Delta P_e^L \quad \forall e \in \Omega_{EN} \tag{41}$$

where N^M, N^D, and N^E are the total numbers of MEGs, MESSs, and EBs, respectively; P_e^M, P_e^D, and P_e^E are the real power outputs of MEGs, MESSs, and EBs, respectively; $\bar{x}$ is the upper limit of variable x; Ω_{EN} is the set of high-voltage substation nodes; and Ω_{ENE} is the set of high-voltage substation nodes into which EBs can integrate.

Constraints (34)-(36) restrict the total number of allocated MPSs in the UPN. Constraints (37)-(39) enforce the lower limit and upper limit of the MPS group that is dispatched in each MVD network. Then, this group of MPSs can be further dispatched to the service transformers in this MVD network. Detailed method is beyond the scope of this paper and can be found in [11]. There is no need to consider the multi-time step in the problem of pre-disaster allocation of MPSs. Besides, MESs and EBs are considered to be fully charged before the dispatch. Constraint (40) enforces that the load loss value after MPS deployment is the expected load loss minus the active power output of the MPS deployment. Constraint (41) indicates that the MPS output of each node does not exceed the expected value of node load loss, because the capacity of emergency power resources is usually less than needed after the extreme weather events.

V. Numerical Study

This section presents case studies on a practical UPN. The optimization model is a mixed-integer linear program and can be directly solved by the existing solver. The computational tasks are performed on a personal laptop computer with an Intel Core i7 Processor (2.20 GHz) and 16 GB RAM, and the code is implemented via the MATLAB-based IBM ILOG CPLEX Optimization Studio V12.8.0.

A. Description of Test Case

A layout of a practical UPN is shown in Fig. 9. The system corresponds to a coastal city in South China with a population of 1.6 million. The system consists of 37 substation nodes, including 2 EHV substations (nodes 36 and 37), 6 HVT substations, and 29 HVD substations. The schematic diagram of a typical MVD network is shown in the green part of the 27-node connection. There are 3 feeders in Fig. 9, and each feeder is connected to one substation or two substations with a normally-open SS. The yearly peak load is 1.271 GW. In this case, the moving track of the typhoon is assumed as follows: the typhoon center reaches the city from the coordinate (0, 0), the moving angle is 45° north of east, and the moving speed is 15 km/hour. Considering that the capacity of MPSs is limited, we assume that the numbers of MEGs, MESs, and EBs are 100, 200, and 1000, respectively. The total active power available from MPSs in the region is 245 MW, of which 45 MW is for MEGs, 100 MW is for MESs, and 100 MW is for EBs. All MPSs are utilized except EBs, which can only be deployed at fixed nodes {1, 6, 10, 15, 19, 28, 32}.

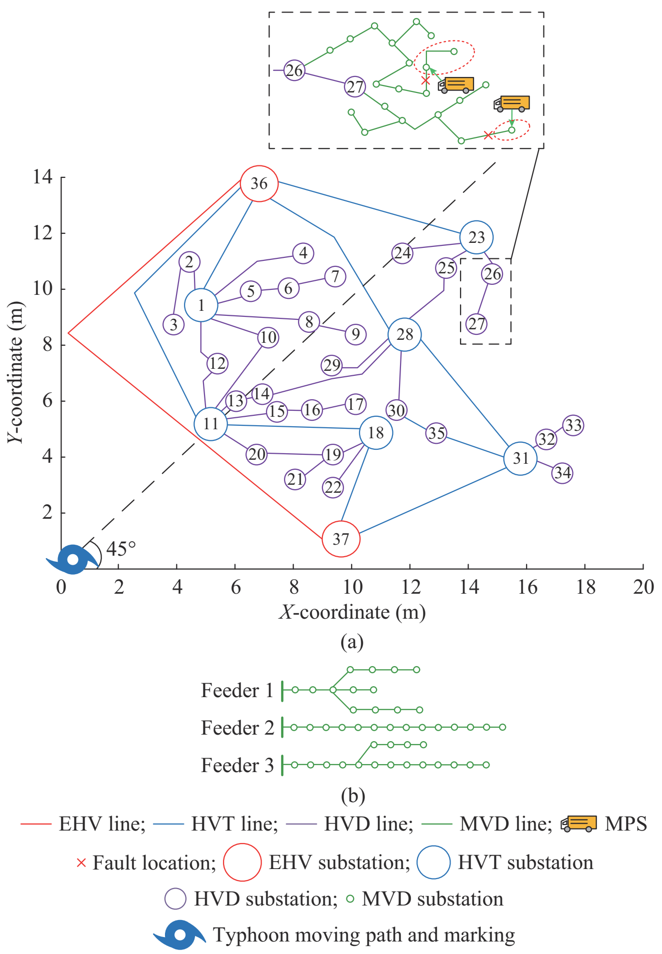

Fig. 9. Layout of a practical UPN. (a) Typical power network topology of HVT and HVD network. (b) Typical power network topology of MVD network.

EHV substations with high importance level and protection measures have low fault probability. Thus, we assume that they will not fail in extreme weather. This subsection only discusses the load loss of nodes 1-35 and the layout of MPS.

B. Simulation Result

1) Expected Load Loss in MVD Network

The fault probability of overhead line is related to the maximum wind speed. According to the typhoon direction, the maximum wind speed within the supply area of each substation node is forecasted, as shown in Fig. 10.

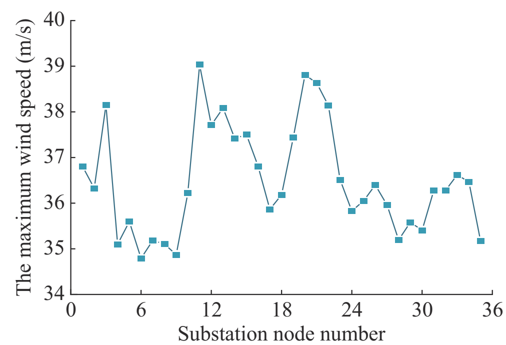

Fig. 10. The maximum wind speed of each substation node.

The maximum wind speed of each substation node in the area ranges from 34.8 to 39.1 m/s, as shown in Fig. 10. Among all substation nodes, node 6 has the smallest wind speed because it is on the moving path of the typhoon eye. Taking the distribution feeders of node 27 as an example, the fault probability of each branch is calculated, as shown in Fig. 11, which is below 0.04. The expected load losses of feeders 1-3 are 967.37 kW, 1401.01 kW, 160.01 kW, respectively. Feeder 3 is supplied by two substations (with one backup), and its load loss expectation is much smaller than those of other two feeders.

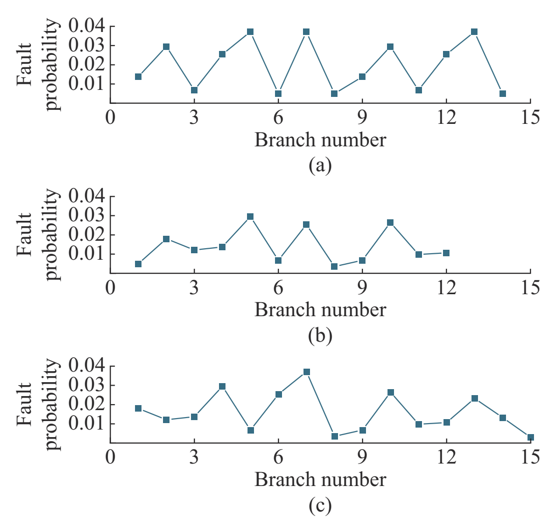

Fig. 11. Fault probability of typical feeders. (a) Feeder 1. (b) Feeder 2. (c) Feeder 3.

The expected load loss caused by the fault of the MVD network is calculated, as shown in Fig. 12. Node 20 has the largest expected load loss of 10.60 MW, and node 11 has the largest load loss ratio of 26.03%.

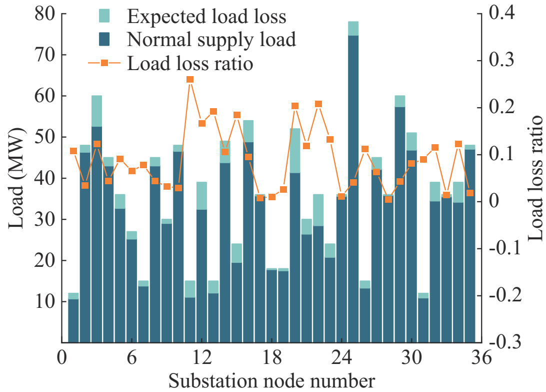

Fig. 12. Expected load loss of MVT substation.

2) Expected Load Loss in HVD Network

As shown in Fig. 9, the EHV substation nodes 36 and 37 are assumed not to be faulted.

Nodes {1, 11, 18, 23, 28, 31} are HVT substation nodes and the other nodes are HVD substation nodes. The calculated fault probabilities of HVT substation to EHV substation are 0.0683, 0.0037, 0.0026, 0.0683, 0.0064, and 0.0036, respectively. The results obtained by the two-stage path search algorithm are shown in Fig. 13. Since there are two power supply paths between nodes 11, 18, 28, 31 and EHV substation, the fault probability is much smaller those that of nodes 1 and 23.

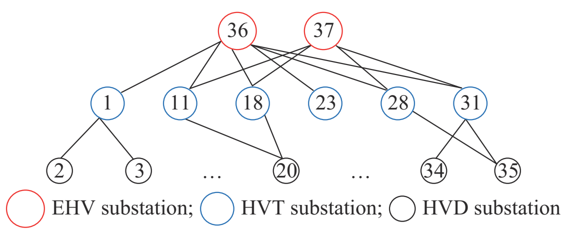

Fig. 13. Results obtained by two-stage path search algorithm.

The results of fault probability are shown in Fig. 14. The expected load losses of HVT and MVT substations are shown in the Fig. 15. In the absence of MPS, the total load losses value is 182.50 MW. The expected load losses of HVT and MVT substations are 78.97 MW and 103.53 MW, respectively.

The total cost of MPSs carried out by the method described in Section IV is 1.012×10^6 RMB. Besides, the solution time is approximately 5 s and the total calculation time is approximately 10 s. The typical voltage level of UPN is shown in Table II.

All MPSs are utilized except EBs, which can only be deployed at fixed nodes {1, 6, 10, 15, 19, 28, 32}, and these nodes have a load loss of 0. By deploying MPSs, the load loss in this area is reduced to 15.18 MW. Although the load losses of nodes 27 and 30 are large, they are interruptible loads.

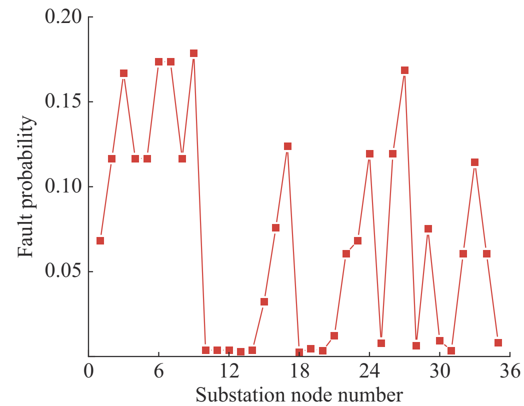

Fig. 14. Results of fault probability.

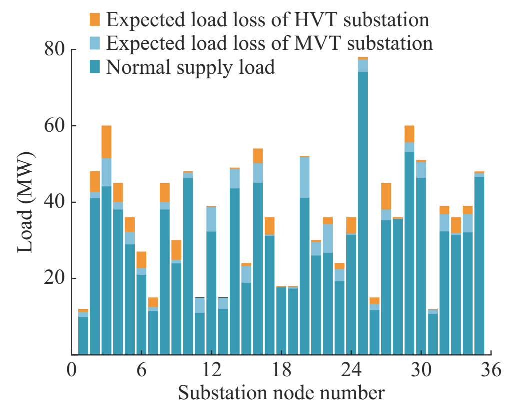

Fig. 15. Expected load loss of HVT and MVT substations.

C. Discussion

The analytical model of expected load loss serves as a tool for the decision makers to identify vulnerable MVD networks and to pre-allocate emergency resources for the upcoming typhoon event and a guidance for preventive action. The accuracy of the load loss is determined by the forecast of disaster intensity and the empirical fragility model of components. Due to the multi-dimensional uncertainty of extreme weather events and the individual difference of UPN components, there are some errors in the estimation. However, the errors can be minimized in the future if a more detailed forecast information of typhoon and flood is available.

VI. Conclusion

This paper establishes analytical modeling of disaster-induced load loss for preventive allocation of MPSs in UPNs. First, an analytical model of the expected load loss of MVD network is constructed. In particular, a two-stage path search algorithm is used to calculate the expected load loss of HVD network. Second, a pre-disaster allocation method of MPSs is proposed for large-scale UPN with the minimization of expected load loss. The following conclusions can be made according to the case studies.

1) The analytical estimation method of load loss effectively combines typhoon prediction data, component fault probability model, and power network topology.

TABLE II
TYPICAL VOLTAGE LEVEL OF UPN

No.	α_e^M	β_e^D	γ_e^E	P_e^M	P_e^D	P_e^E	ΔP_e^L
1	0	0	21	0	0	2.03	0
2	18	3	0	5.40	1.5	0	0.02
3	1	31	0	0.30	15.5	0	0.01
4	6	10	0	1.80	5.0	0	0.06
5	8	9	0	2.40	4.5	0	0.11
6	0	0	60	0	0	5.97	0
7	5	4	0	1.48	2.0	0	0
8	4	11	0	1.20	5.5	0	0.16
9	0	10	0	0	5.0	0	0.96
10	0	0	16	0	0	1.60	0
11	2	6	0	0.60	3.0	0	0.31
12	0	13	0	0	6.5	0	0.13
13	0	5	0	0	2.5	0	0.38
14	0	10	0	0	5.0	0	0.34
15	0	0	51	0	0	5.05	0
16	29	0	0	8.70	0	0	0.12
17	9	4	0	2.70	2.0	0	0
18	1	0	0	0.23	0	0	0
19	0	0	6	0	0	0.56	0
20	0	21	0	0	10.5	0	0
21	8	3	0	2.39	1.5	0	0
22	1	17	0	0.30	8.5	0	0.42
23	12	2	0	3.60	1.0	0	0
24	10	3	0	3.00	1.5	0	0.04
25	1	7	0	0.30	3.5	0	0
26	4	4	0	1.20	2.0	0	0.01
27	4	1	0	1.20	0.5	0	7.98
28	0	0	5	0	0	0.40	0
29	1	13	0	0.30	6.5	0	0.06
30	2	0	0	0.60	0	0	3.95
31	2	1	0	0.60	0.5	0	0.02
32	0	0	66	0	0	6.58	0
33	15	0	0	4.50	0	0	0.05
34	6	10	0	1.80	5.0	0	0.05
35	1	2	0	0.29	1.0	0	0
Total	150	200	225	44.89	100.0	22.19	15.18

It serves as the theoretical basis for the optimal MPS allocation for resilience enhancement.

2) The preventive allocation of MPS realizes the optimal utilization of limited power supply resources, prioritizes the power supply of important loads, and reduces the expected load loss.

In addition, the analytical models established for MVT and HVD networks greatly reduce the computational workload, which is essential in the application scenario of strict computation time.

REFERENCES

[1] J. Li, Y. Xu, Y. Wang, *et al*., "Resilience-motivated distribution system restoration considering electricity-water-gas interdependency," *IEEE Transactions on Smart Grid*, vol. 12, no. 6, pp. 4799-4812, Nov. 2021.

[2] President's Council of Economic Advisers & U.S. Dept. Energy's Office of Electricity & Energy Reliability. (2013, Jun.). Economic benefits of increasing electric grid resilience to weather outages. [Online]. Available: https://www. energy. gov/articles/economic-benefits-increasing-electric-grid-resilience-weather-outages

[3] Electric Power Research Institute. (2013, Jan.). Enhancing distribution resiliency: opportunities for applying innovative technologies. [Online]. Available: https://www.epri.com/research/products/000000000001026889

[4] Z. Tao and L. Han, "Emergency response, influence and lessons in the 2021 compound disaster in Henan Province of China," *International Journal of Environmental Research and Public Health*, vol. 19, no. 1, pp. 483-488, Jan. 2022.

[5] J. W. Busby, K. Baker, M. D. Bazilian *et al*., "Cascading risks: understanding the 2021 winter blackout in Texas," *Energy Research & Social Science*, vol. 77, pp. 1-10, Jul. 2021.

[6] Office of Electricity Delivery and Energy Reliability at U.S. Department of Energy. (2015, Sept.). United States electricity industry primer. [Online]. Available: https://www.energy.gov/sites/prod/files/2015/12/f28/united-states-electricity-industry-primer.pdf#page=13&zoom=100,93,172

[7] Electricity Network Strategy Group. (2012, Feb.). Our electricity transmission network: a vision for 2020. [Online]. Available: https://assets. publishing. service. gov. uk/government/uploads/system/uploads/attachment_data/file/48275/4264-ensg-summa ry.pdf.

[8] A. Abessi and S. Jadid, "Internal combustion engine as a new source for enhancing distribution system resilience," *Journal of Modern Power Systems and Clean Energy*, vol. 9, no. 5, pp. 1130-1136, Sept. 2021.

[9] B. Taheri, A. Safdarian, M. Moeini-Aghtaie *et al*., "Distribution system resilience enhancement via mobile emergency generators," *IEEE Transactions on Power Delivery*, vol. 36, no. 4, pp. 2308-2319, Aug. 2021.

[10] A. Arif, Z. Wang, J. Wang *et al*., "Power distribution system outage management with co-optimization of repairs, reconfiguration, and DG dispatch," *IEEE Transactions on Smart Grid*, vol. 9, no. 5, pp. 4109-4118, Sept. 2018.

[11] Q. Shi, H. Wan, W. Liu *et al*., "Preventive allocation and post-disaster cooperative dispatch of emergency mobile resources for improved distribution system resilience," *International Journal of Electrical Power & Energy Systems*, vol. 152, pp. 1-13, Oct. 2023.

[12] W. Yuan, J. Wang, F. Liu *et al*., "Robust optimization-based resilient distribution network planning against natural disasters," *IEEE Transactions on Smart Grid*, vol. 7, no. 6, pp. 2817-2826, Nov. 2016.

[13] X. Wang, M. Shahidehpour, C. Jiang *et al*., "Resilience enhancement strategies for power distribution network coupled with urban transportation system," *IEEE Transactions on Smart Grid*, vol. 10, no. 4, pp. 4068-4079, Jul. 2019.

[14] S. Ma, S. Li, Z. Wang *et al*., "Resilience-oriented design of distribution systems," *IEEE Transactions on Power Systems*, vol. 34, no. 4, pp. 2880-2891, Jul. 2019.

[15] Q. Shi, F. Li, T. Kuruganti *et al*., "Resilience-oriented DG siting and sizing considering stochastic scenario reduction," *IEEE Transactions on Power Systems*, vol. 36, no. 4, pp. 3715-3727, Jul. 2021.

[16] H. Chen, J. Wang, J. Zhu *et al*., "A two-stage stochastic mixed-integer programming model for resilience enhancement of active distribution networks," *Journal of Modern Power Systems and Clean Energy*, vol. 11, no. 1, pp. 94-106, Jan. 2023.

[17] S. Lei, J. Wang, C. Chen *et al*., "Mobile emergency generator pre-positioning and real-time allocation for resilient response to natural disasters," *IEEE Transactions on Smart Grid*, vol. 9, no. 3, pp. 2030-2041, May 2018.

[18] Q. Zhang, Z. Wang, S. Ma *et al*., "Stochastic pre-event preparation for enhancing resilience of distribution systems," *Renewable and Sustainable Energy Reviews*, vol. 152, pp. 1-13, Dec. 2021.

[19] H. Gao, Y. Chen, S. Mei *et al*., "Resilience-oriented pre-hurricane resource allocation in distribution systems considering electric buses," *Proceeding of the IEEE*, vol. 105, no. 7, pp. 1214-1233, Jul. 2017.

[20] C. Wang, T. Zhang, F. Luo *et al*., "Fault incidence matrix based reliability evaluation method for complex distribution system," *IEEE Transactions on Power Systems*, vol. 33, no. 6, pp. 6736-6745, Nov. 2018.

[21] R. Cheng, N. Shi, S. Maharjan *et al*., "Automatic self-adaptive local voltage control under limited reactive power," *IEEE Transactions on Smart Grid*, vol. 14, no. 4, pp. 2851-2862, Jul. 2023.

[22] Q. Shi, W. Liu, B. Zeng *et al*., "Enhancing distribution system resilience against extreme weather events: concept review, algorithm summary, and future vision," *International Journal of Electrical Power &*

Energy Systems, vol. 138, pp. 1-13, Jun. 2022.
[23] M. Yan, X. Ai, M. Shahidehpour *et al*., "Enhancing the transmission grid resilience in ice storms by optimal coordination of power system schedule with pre-positioning and routing of mobile DC de-icing devices," *IEEE Transactions on Power Systems*, vol. 34, no. 4, pp. 2663-2674, Jul. 2019.
[24] H. T. Nguyen, J. Muhs, and M. Parvania, "Preparatory operation of automated distribution systems for resilience enhancement of critical loads," *IEEE Transactions on Power Delivery*, vol. 36, no. 4, pp. 2354-2362, Aug. 2021.
[25] Y. Sang, J. Xue, M. Sahraei-Ardakani, "An integrated preventive operation framework for power systems during hurricanes," *IEEE System Journal*, vol. 14, no. 3, pp. 3245-3255, Sept. 2020.
[26] M. Movahednia, A. Kargarian, and C. E. Ozdemir, "Power grid resilience enhancement via protecting electrical substations against flood hazards: a stochastic framework," *IEEE Transactions on Industrial Informatics*, vol. 18, no. 3, pp. 2132-2143, Mar. 2022.
[27] E. L. Barrett, K. Mahapatra, M. Elizondo *et al*., "A risk-based framework for power system modeling to improve resilience to extreme events," *IEEE Open Access Journal of Power & Energy*, vol. 10, pp. 25-35, Jan. 2023.
[28] A. Arab, A. Khodaei, S. K. Khator *et al*., "Stochastic pre-hurricane restoration planning for electric power systems infrastructure," *IEEE Transactions on Smart Grid*, vol. 6, no. 2, pp. 1046-1054, Mar. 2015.
[29] Y. Tian and W. Chen, "Selection principle of neural grounding mode of distribution power network and its fault processing technology in Japan," *Distribution & Utilization*, vol. 34, no. 5, pp. 14-20, May 2017.
[30] U.S. Department of Energy. (2016, Sept.). Distribution system automation: results from the smart grid investment grant program. [Online]. Available: https://www.energy.gov/sites/prod/files/2016/11/f34/Distribution%20Automation%20Summary%20Report_09-29-16.pdf
[31] Y. Wu, Y. Xue, H. Wang *et al*., "Extension of power system early-warning defense schemes by integrating typhoon information," in *Proceedings of International Conference on Sustainable Power Generation and Supply*, Hangzhou, China, Sept. 2012, pp. 1-7.
[32] S. Zhang, Y. He, J. Cai *et al*., "A new method based on Monte Carlo simulation for reliability evaluation of distribution network considering the influence of typhoon," in *Proceedings of International Conference on Power System Technology*, Guangzhou, China, Nov. 2018, pp. 3341-3346.
[33] Y. Chen, S. Wang, B. Chen *et al*., "Evaluation of the failure probability of power transmission corridors during typhoons using digital elevation information," *Power System Technology*, vol. 42, no. 7, pp. 2295-2302, Jul. 2018.
[34] M. Panteli, C. Pickering, S. Wilkinson *et al*., "Power system resilience to extreme weather: fragility modeling, probabilistic impact assessment, and adaptation measures," *IEEE Transactions on Power Systems*, vol. 32, no. 5, pp. 3747-3757, Sept. 2017.
[35] W. Huang, N. Liu, J. Wang *et al*., "A risk assessment method and early warning system for substation under heavy rainfall," China, Patent 111738617, Jul. 1, 2020.
[36] R. C. Agarwal, C. C. Aggarwal, and V. V. V. Prasad, "A tree projection algorithm for generation of frequent item sets," *Journal of Parallel and Distributed Computing*, vol. 61, no. 3, pp. 350-371, Mar. 2001.

Zhuorong Wang received the B.S. degree in Taiyuan University of Technology, Taiyuan, China, in 2021. She is now pursuing the M.Sc. degree in the School of Electrical and Electronic Engineering, North China Electric Power University, Beijing, China. Her research interests include resilient urban power system and power system restoration.

Qingxin Shi received the B. S. degree in Zhejiang University, Hangzhou, China, in 2011, the M.Sc. degree in University of Alberta, Edmonton, Canada, in 2014, and the Ph. D. degree in The University of Tennessee, Knoxville, USA, in 2019, where he worked as a Research Assistant Professor from 2019 to 2020. Currently, he is an Assistant Professor in the School of Electrical and Electronic Engineering, North China Electric Power University, Beijing, China. His research interests include demand response, frequency regulation, and resilient urban power system.

Ke Fan received the B.S. degree in North China Electric Power University, Beijing, China, in 2021. He is now pursuing the M.Sc. degree in the School of Electrical and Electronic Engineering, North China Electric Power University. His research interests include frequency regulation and power system operation with high renewable energy penetration.

Haiteng Han received the B.S. and Ph.D. degrees in Southeast University, Nanjing, China, in 2010 and 2019, respectively. He is currently an Assistant Professor in the College of Energy and Electrical Engineering, Hohai University, Nanjing, China. His research interests include power system security assessment, demand response, and electricity market.

Wenxia Liu received the B.S. degree in radio technology from Nanjing University of Science and Technology, Nanjing, China, in 1990, and M.S. and Ph. D. degrees in electrical engineering and automation from Northeast of China Electrical Power University in 1995 and 2009, respectively. She is currently Professor in the School of Electrical and Electronic Engineering, North China Electrical Power University, Beijing, China. Her research interests include risk assessment in power system, power system dispatch, and management automation.

Fangxing (Fran) Li received the B. S. E. E. and M. S. E. E. degrees from Southeast University, Nanjing, China, in 1994 and 1997, respectively, and the Ph. D. degree from Virginia Polytechnic Institute and State University, Blacksburg, USA, in 2001. Currently, he is the James McConnell Professor at The University of Tennessee (UT), Knoxville, USA. His research interests include renewable energy integration, demand response, electricity market, power system control, and power system computing.